Whole transcriptome profiling of placental pathobiology in SARS-CoV-2 pregnancies identifies placental dysfunction signatures.

Nataly Stylianou[1#], Ismail Sebina[2#], Nicholas Matigian[3], James Monkman[2], Hadeel Doehler[1], Joan Röhl[4], Mark Allenby[5], Andy Nam[6], Liuliu Pan[6], Anja Rockstroh[1], Habib Sadeghirad[2], Kimberly Chung[2], Thais Sobanski[1], Ken O'Byrne[1], Ana Clara Simoes Florido Almeida[7], Patricia Zadorosnei Rebutini[7], Cleber Machado-Souza[8], Emanuele Therezinha Schueda Stonoga[9], Majid E Warkiani[10], Carlos Salomon[11], Kirsty Short[12], Lana McClements[10], Lucia de Noronha[7], Ruby Huang[13], Gabrielle T. Belz[2], Fernando Souza-Fonseca-Guimaraes[2], Vicki Clifton[14], Arutha Kulasinghe[2*].

[1] *Centre for Genomics and Personalised Health, School of Biomedical Sciences, Queensland University of Technology, Brisbane, QLD 4102, Australia*

[2] *Frazer Institute, Faculty of Medicine, The University of Queensland, Brisbane, QLD 4102, Australia.*

[3] *QCIF Bioinformatics, St Lucia, QLD 4102, Australia*

[45] *Faculty of Health Sciences and Medicine, Bond University, Queensland, Australia*

[5] *BioMimetic Systems Engineering Lab, School of Chemical Engineering, University of Queensland (UQ), St Lucia, QLD, Australia*

[6] *Nanostring Technologies, Inc, Seattle, WA, USA*

[7] *Postgraduate Program of Health Sciences, School of Medicine, Pontifícia Universidade Católica do Paraná´-PUCPR, Curitiba, Brazil.*

[8] *Postgraduate Program in Biotechnology Applied in Health of Children and Adolescent, Instituto de Pesquisa Pelé Pequeno Príncipe, Faculdades Pequeno Príncipe, Curitiba, Brazil*

[9] *Department of Medical Pathology, Clinical Hospital, Universidade Federal do Paraná´-UFPR, Curitiba, Brazil.*

[10] *School of Life Sciences & Institute for Biomedical Materials and Devices, Faculty of Science, University of Technology Sydney, NSW, Australia.*

[11] *Exosome Biology Laboratory, Centre for Clinical Diagnostics, University of Queensland Centre for Clinical Research, Royal Brisbane and Women's Hospital, Faculty of Medicine, The University of Queensland, Brisbane, Australia.*

[12] *School of Chemistry and Molecular Biosciences, Faculty of Science, The University of Queensland, St Lucia QLD 4067, Australia.*

[13] *School of Medicine, College of Medicine, National Taiwan University, Taipei, Taiwan.*

[14] *Mater Medical Research Institute – University of Queensland, Brisbane, Australia.*

 # These authors contributed equally

*Correspondence: Dr Arutha Kulasinghe, Frazer Institute, Faculty of Medicine, The University of Queensland. 37 Kent Street, Woolloongabba, Queensland 4012, Australia. E: arutha.kulasinghe@uq.edu.au

Graphical abstract: In this study, using spatial digital profiling transcriptomic approaches, we demonstrate that SARS-CoV-2 infection in pregnancy disrupts optimal placental function by altering the genomic architecture of trophoblasts and villous core stromal cells.

ABSTRACT

Objectives: Severe Acute Respiratory Syndrome Coronavirus 2 (SARS-CoV-2) virus infection in pregnancy is associated with higher incidence of placental dysfunction, referred to by a few studies as a “preeclampsia-like syndrome”. However, the mechanisms underpinning SARS-CoV-2-induced placental malfunction are still unclear. Here, we

investigated whether the transcriptional architecture of the placenta is altered in response to SARS-CoV-2 infection.

Methods: We utilized whole-transcriptome, digital spatial profiling, to examine gene expression patterns in placental tissues from participants who contracted SARS-CoV-2 in the third trimester of their pregnancy (n=7) and those collected prior to the start of the coronavirus disease 2019 (COVID-19) pandemic (n=9).

Results: Through comprehensive spatial transcriptomic analyses of the trophoblast and villous core stromal cell subpopulations in the placenta, we identified signatures associated with hypoxia and placental dysfunction during SARS-CoV-2 infection in pregnancy. Notably, genes associated with vasodilation (*NOS3*), oxidative stress (*GDF15*, *CRH*), and preeclampsia (*FLT1, EGFR, KISS1, PAPPA2)*, were enriched with SARS-CoV-2. Pathways related to increased nutrient uptake, vascular tension, hypertension, and inflammation, were also enriched in SARS-CoV-2 samples compared to uninfected controls.

Conclusions: Our findings demonstrate the utility of spatially resolved transcriptomic analysis in defining the underlying pathogenic mechanisms of SARS-CoV-2 in pregnancy, particularly its role in placental dysfunction. Furthermore, this study highlights the significance of digital spatial profiling in mapping the intricate crosstalk between trophoblasts and villous core stromal cells, thus shedding light on pathways associated with placental dysfunction in pregnancies with SARS-CoV-2 infection.

KEYWORDS: Placental dysfunction, SARS-CoV-2, COVID-19, digital spatial profiling, gene expression profiling, trophoblasts, villous core stroma.

INTRODUCTION

Viral infections in pregnancy can disrupt placental function and predispose pregnancy complications, including late-onset preeclampsia, preterm birth, stillbirth, and intrauterine fetal demise[1-4]. Recent studies have revealed that pregnant women who contract Severe Acute Respiratory Syndrome Coronavirus 2 (SARS-CoV-2, which causes coronavirus disease 2019 [COVID-19]), can experience placental dysfunction and what has been referred to as "preeclampsia-like syndrome" [5-10]. Placental tissues from COVID-19 patients exhibit increased vasculopathy and inflammation, which are characteristic pathological features of preeclampsia [11]. Moreover, clinical manifestations observed in COVID-19 patients, such as COVID-19-associated hypoxia, hypertension, endothelial dysfunction, kidney disease, thrombocytopenia, and liver injury, overlap with those observed in preeclampsia[5, 12]. However, mechanisms through which SARS-CoV-2 infection predisposes pregnancies to these preeclampsia-like pathological features are largely unclear.

The placenta is vital for fetal development and growth throughout gestation as it is a functional interface between the mother and fetus[13]. This interface comprises various anatomically distinct sites, including the decidua basalis, where maternal immune cells and decidual stromal cells interact with fetal extravillous trophoblasts[14]. The maternal-fetal interface also consists of the placental intervillous space, where maternal immune cells interact with fetal syncytiotrophoblasts, and the boundary between the parietalis and the chorion laeve in the chorioamniotic membranes[14]. Other cell types within this interface, such as villous cytotrophoblasts, column cytotrophoblasts, fibroblasts, endothelial cells, and Hofbauer cells, contribute to nutrient and waste exchange, hormone production, protection from pathogens, and maternal immune responses essential for fetal development [13, 14].

Whether SARS-CoV-2 infection modifies the transcriptomic architecture and functional characteristics of different cell types within these distinct placental sites is still unclear.

In this study, we utilised digital spatial whole-transcriptomic analysis of human placental tissue to delineate molecular pathways associated with SARS-CoV-2 infection-induced placental pathology in pregnancy. Specifically, we focused our analysis on defining the distinct transcriptional profiles of trophoblasts and villous core stromal cell populations (the latter including endothelial, fibroblast, and immune cells), in the context of SARS-CoV-2 infection. We identified several pivotal pathways that underlie the development of a "preeclampsia-like syndrome" associated with SARS-CoV-2 infection in pregnancy.

RESULTS

Characterization of patient demographics and histopathology in collected placentae.

Tissue microarrays were constructed using placental cores that were collected immediately after birth from unvaccinated participants who had tested positive within 15 days prior to delivery (Alpha strain, April 2020, n=7), and unvaccinated participants who were negative for SARS-CoV-2 throughout their pregnancy (n=9; Table 1). There were no significant differences in placental weight, fetal weight, gestational age, comorbidities, or maternal age between the two groups (Table 1). Within the SARS-CoV-2 group, 3/7 newborns were born preterm, compared to 4/9 in the control group (Table 1).

No SARS-CoV-2 viral load was detected in the placental cores from the SARS-CoV-2 infected group through examination by RNAscope of the SARS-CoV-2 spike mRNA (data not shown). With the aid of a trained placental pathologist, an area featuring an anchoring

villus, and an area featuring a cluster of terminal villi, were designated as two areas of interest (AOI) within each placental core (Figure 1a). AOIs where immunofluorescently stained with PanCK to identify trophoblast populations, and vimentin to identify stromal populations (i.e., fibroblasts, endothelial cells). Transcriptional expression was collected separately for PanCK positive and separately for vimentin positive cells within each AOI using the Whole Transcriptome Atlas kit (Nanostring; Figure 1a). Subsequent cell deconvolution was performed to assess the purity of each collection (Figure 1b). As expected, transcriptional expression from PanCK positive regions within the AOIs had high proportion of trophoblast populations, compared to vimentin positive regions that had higher proportions of fibroblast and endothelial cells (Figure 1b-f). Due to the overlapping nature of cells, all samples captured a proportion of immune cell types (macrophages, monocytes, Hofbauer cells), except for the PanCK positive regions that displaying a proportion of granulocytes that was absent from the vimentin positive regions within the AOIs (Figure 1b, g-j). SARS-CoV-2 infection did not significantly alter the transcriptional proportion of any cell type assessed when compared to controls (Figure 1b-j). In subsequent analyses, the PanCK positive regions within the AOIs will be referred to as “Trophoblasts” and the vimentin positive regions will be referred to as “Villous Core Stroma” compartments, due to the predominant enriched cell type they represent.

SARS-CoV-2 infection related pathways enriched in the placenta despite absence of detectable viral particles.

Unsupervised clustering of the normalised gene counts by principal component analysis showed that SARS-CoV-2 samples clustered separately to control samples in dimension 1, and further by phenotype in dimension 2, supporting that infection with SARS-CoV-2 markedly alters the transcriptional profiles of the trophoblast and villous core stroma cell populations (Figure 2a-b). Notably, there was very high overlap of genes differentially

expressed between the anchoring and the terminal villi; for instance, trophoblasts at the anchoring villi had 1,791 differentially expressed genes versus 493 at the terminal villi, with 405 genes in common between them (82% overlap; Supplementary table 1, Figure 2c). Similarly, the villous core stroma cells at the anchoring villi had 1,139 differentially expressed genes versus 601 at the terminal villi, with 458 genes in common between them (76% overlap; Supplementary table 1, Figure 2c). As expected, there was minimal overlap in differential gene expression between the trophoblasts and villous core stroma compartments, which highlights their distinct cell phenotypes (Figure 2c).

Despite the SARS-CoV-2 samples showing undetectable SARS-CoV-2 by RNA-scope, transcriptional profiling showed positive enrichment of SARS-CoV-2 related pathways in the SARS-CoV-2 samples, such as "SARS_COV_2_INFECTION", and "SARS_COV_2_HOST_INTERACTIONS" from the Reactome database, as well as the Interferon Alpha Response pathway from the Hallmark database, which is a first-line immune response pathway that has been associated with SARS-CoV-2 infection (Figure 2d-f)[15] . These pathways were supported by increased expression of genes that have been associated with SARS-CoV-2, such as the inflammatory marker *IFI16*[16], disease progression marker *IFI27*[17], disease prognosticator *B2M*[18], activation of Janus Kinases (i.e., *JAK1*), and expression of *STAT3*[19] (Figure 2 g-j). Notably, gene expression for these markers was elevated predominantly in the villous core stroma cell compartment, presumably stemming from the immune subpopulation within the stroma. Indeed, specific analysis of the villus core stroma compartment revealed enrichment of several immune related pathways from the Hallmarks database such as IL6/JAK/STAT3 signalling, IL2/STAT5 signalling, TNF-alpha signalling, inflammatory response, and complement pathways (Figure 3a), supporting that the immune cells within the placental villi are actively responding to SARS-CoV-2 infection.

SARS-CoV-2 infection enriches hypoxia and placental dysfunction pathways.

Pathway enrichment analysis of the genes differentially expressed in response to SARS-CoV-2 infection, revealed pathways related to placental disfunction, in both the trophoblast and villous core stroma compartments. For instance, hypoxia and oxidative phosphorylation pathways were enriched in the villous core stroma (Figure 3a), both of which have been previously linked with placental dysfunction and increased incidence of developing preeclampsia[20]. Hypoxia triggers TGF-β signalling and angiogenesis [21], and both TGF- β signalling and angiogenesis related pathways were enriched in the villous core stroma in response to SARS-CoV-2 infection (Figure 3b). Furthermore, pathways related to haemorrhage were upregulated and pathways related to vascular tension, such as hyperaldosteronin/renin pathways, acetylcholine channels, and olfactory receptors, were downregulated in the villous core stroma (Figure 3b). Trophoblast cells exhibited enrichment of pathways related to nitric oxide production (Figure 3c), which is a potent vasodilator[22]. Conversely, pathways related to calcium import[23] and vasoconstriction were downregulated in trophoblasts (Figure 3c), supporting the notion that the placenta actively reduces vascular tension during SARS-CoV-2 infection. In parallel, trophoblasts showed an increase in cell-cell adherence, communication, and transmembrane amino acid transport, including MTORC1 signalling[24], suggesting that nutritional uptake to the foetus is enhanced in response to SARS-CoV-2 infection (Figure 3a and 3c). Further, pathways related to allograft rejection and MHC molecules were decreased, suggestive of a defensive mechanism by the trophoblast layer to protect gestation (Figure 3a and 3c).

Markers associated with preeclampsia are elevated with SARS-CoV-2

Placentae from the SARS-CoV-2 group showed several markers that have been previously associated with hypoxia and placental dysfunction. For instance, the hypoxia and preeclampsia associated markers Fms Related Receptor Tyrosine Kinase 1 (*FLT1)* , *FLT4*, epidermal growth factor receptor (*EGFR),* and pappalysin-2 (*PAPPA2*) were increased in

trophoblasts from the SARS-CoV-2 group (Figure 3e-i)[25-28]. Additionally, markers associated with placental dysfunction and oxidative stress such as Nitric oxide synthase 3 (*NOS3*)[29], corticotrophin-releasing hormone (*CRH*)[30], kisspeptin 1 (*KISS1*)[31], Growth Differentiation Factor 15 (*GDF15*)[32], and tissue factor pathway inhibitor 2 (*TFPI-2*)[33], were also elevated in the trophoblasts from the SARS-CoV-2 group (Figure 3e, 3j-k). Transforming growth factor b1 (*TGFβ-1*), and the PAPP-A2 substrates *IGFBP4/5* (Figure 3d and 3l), were also elevated in the villous core stroma, both markers associated with increased preeclampsia risk[21, 34].

Given that a number of these pathways and genes are associated with preeclampsia, as well as several recent studies reporting SARS-CoV-2 in predisposing pregnant individuals to preeclampsia[5-10], we next assessed the enrichment of a preeclampsia-specific gene set generated from published patient cohorts[35]. The gene set was generated by Moslehi et al., where they found 419 genes to be common between four studies examining preeclampsia versus healthy pregnancies[35]. These 419 genes are involved in pathways relevant to preeclampsia, such as oxidative stress, hypoxia, and immune response[35-37]. In our data, this preeclampsia signature was positively enriched in patient samples from the SARS-CoV-2 group (NES 3.49, FDR <0.001; Figure 3m), which aligns with the positive enrichment of hypoxia, immune, and oxidative stress, related pathways we observed in our studies (Figure 3a).

DISCUSSION

Using digital spatial profiling, we quantified the expression of key markers within distinct cellular compartments of the placenta, providing a detailed picture of the molecular changes occurring in response to SARS-CoV-2 infection. Although our study is limited by its

relatively small cohort, cross-sectional nature, and low availability of clinical data, it offers valuable insights into the interplay between trophoblasts and the cells within the villous core stroma in the placenta and how this relationship is influenced by SARS-CoV-2 infection. Close examination of the transcriptional alterations occurring in the placental trophoblast and villous core stroma in response to SARS-CoV-2, revealed a notable number of genes that are enriched in biological pathways previously associated with placental dysfunction.

Trophoblasts from the SARS-CoV-2-infected group had significantly higher levels of *NOS3* compared to the control group (Figure 3j). The upregulation of NOS3 is associated with increased endogenous production of the vasodilator nitric oxide, as a response to altered vascular reactivity, endothelial dysfunction, and hypertension[22, 38]. Interestingly, NOS has been previously found to be highly upregulated to supraphysiological levels in animal models of infection-mediated inflammation during pregnancy, leading researchers to hypothesise that increased NOS may play a role in placental inflammation[39-41]. In response to increased NOS by the trophoblasts, the villous core stromal showed increased expression in biological pathways related to systemic pressure and vasodilation. This included the downregulation of olfactory receptors, acetylcholine channels, and hyperaldosteronin/renin pathways, alongside upregulated hypoxia pathways, suggesting deregulation of the vascular tone and blood pressure due to a hypoxic environment[42].

Additional transcriptional analysis of trophoblast and villous core stromal compartments from SARS-CoV-2-infected samples identified several transcriptional variations that have been previously associated with preeclampsia (Figure 3). Trophoblasts had higher expression of *EGFR*, a marker that increases with hypoxia and is known to upregulate *FLT1*, where

241 excessive release of soluble FLT1 by syncytiotrophoblasts is a characteristic marker of late
242 onset preeclampsia[43]. There was prominent increase of *PAPPA2* in the trophoblasts, the
243 latter considered to become upregulated in response to hypoxia, and placental pathologies,
244 including preeclampsia[44]. Notably, the PAPPA2 substrates IGFBP4 and IGFBP5 were
245 concurrently upregulated in the villous core stromal compartment, whereby the interaction of
246 PAPPA2 with IGFBP4/5 increases levels of IGF2, which was also increased in the villous
247 core stromal cells in the SARS-CoV-2-infected group (Figure 3d)[34]. Additionally, the villous
248 core stromal compartment had decreased levels of Isthmin-2 (*ISM2*), a placental marker that
249 is downregulated with preeclampsia[45]. *GDF15*, *TFPI-2*, *KISS1*, and *CRH* genes were also
250 upregulated in SARS-CoV-2-infected trophoblasts, all previously associated with placental
251 oxidative stress, hypertension, and preeclampsia[34, 46-48].

252 In conclusion, our data suggest that the placenta from pregnancies with SARS-CoV-2 adopts
253 a transcriptional profile aligning with placental dysfunction that has been observed in
254 pregnant participants who develop 'preeclampsia-like' syndrome. Using digital spatial
255 profiling, our studies showcased the crosstalk between the trophoblast and villous core
256 stromal cell populations, and how this is enriched with pathways associated with placental
257 dysfunction. Our findings set the foundation for a more comprehensive understanding of
258 placental dysfunction in pregnant individuals with SARS-CoV-2 infection and offer
259 important insights into the potential mechanisms through which SARS-CoV-2 may impact
260 pregnancy outcomes and fetal development.

261

262 **METHODS**

263 **Study Design**

The SARS-CoV-2 group (n=7) consisted of pregnant, unvaccinated participants, who were symptomatic with COVID-19 in their third trimester (confirmed by RT-qPCR from nasopharyngeal swabs). Placental tissue samples were collected at birth at the Hospital de Clínicas (HC) and Hospital Nossa Senhora das Graças, Brazil, with ethics approval from the National Commission for Research Ethics (CONEP) under approval number 30188020.7.1001.0020[49]. The control group was comprised of archived placentae from nine COVID19-negative people collected during delivery at the Complexo Hospital de Clínicas, Universidade Federal do Paraná, Curitiba, Brazil between 2016 and 2018. To account for maternal co-morbidities, maternal age, and gestational age, the control group was selected to match these clinical features as presented in the SARS-CoV-2 group. Participant cohort and their clinical characteristics are summarised in Table 1. Morphological analysis was performed in all placentas from SARS-CoV-2-infected and control groups using the Amsterdam Placental Workshop Group Consensus Statement[50]. Histological sections were systematically identified and evaluated by two experienced pathologists to obtain samples for tissue microarray (TMA) construction, as described in a previous work[49]. Two TMAs were prepared from the placental samples, following the workflow demonstrated in Figure 1.

RNAscope

A serial section from the TMAs (4 um) was incubated with RNAscope probes targeting SARS-CoV-2 spike mRNA (nCoV2019, #848568-C3, ACDBio, CA, USA), as per manufacturer's instructions for automation on Leica Bond RX. DNA was visualised with Syto13 (500 nM, #S7575, ThermoFisher Scientific, MA, USA), and SARS-CoV-2 spike mRNA with TSA Plus CY5 (1:1500, #NEL745001KT, Akoya Biosciences, MA, USA). Fluorescent images were acquired with NanoString GeoMX DSP at 20×.

Digital spatial profiling with Nanostring GeoMX platform

TMA slides were freshly sectioned (4 um thick serial sections) and prepared according to the Nanostring GeoMX Digital Spatial Profiler (DSP) slide preparation for RNA profiling (NanoString, WA, USA). Slides were hybridised with the NanoString Technologies Whole Transcriptome Atlas (WTA) barcoded probe set (~18,000 genes), followed by fluorescent staining with Pan-Cytokeratin (PanCK, clone AE-1/AE-3, AF488, Santa Cruz NBP2-33200AF488, [2 µg/mL], CA, USA) to identify trophoblasts, vimentin (VIM, clone E-5, AF594, Santa Cruz sc-373717, [1 µg/mL], CA, USA) to identify endothelial and mesenchymal stromal cells, and SYTO83 to identify nuclei. With the aid of a trained placental pathologist, an area featuring an anchoring villus, and an area featuring a cluster of terminal villi, were designated as two areas of interest (AOI) within each placental core. Oligonucleotides linked to hybridized mRNA targets were cleaved separately for PanCK positive regions within each AOI, and separately for vimentin positive regions. Cleaved oligonucleotides were collected for counting using Illumina i5 and i7 dual indexing as described previously[51, 52]. Paired-end sequencing (2□×□75) was performed using an Illumina NextSeq550 up to 400M total aligned reads. Fastq files were processed using the Nanostring DND system and uploaded to the GeoMX DSP system where raw counts were aligned with their respective AOIs.

Data normalisation, differential expression analysis, and pathway enrichment analysis

Raw data were normalised to the 134 negative probes in the Human Whole Transcriptome Atlas probe set followed by upper quantile normalisation using the R package RUVseq[53]. Transcriptional data from PanCK positive regions within each AOI were normalised separately to the vimentin positive regions. Differential gene expression analysis between SARS-CoV-2 positive and negative groups was performed separately for PanCK positive

regions within each AOI, and separately for vimentin positive regions, using the R package limma[54]. Bayesian adjusted t-statistic method was used where foetal sex and TMA slide number were considered as co-variants. A fold change of +/- 1.5 and *P*-value ≤ 0.05 (adjusted for a false discovery rate of 5%) was considered significant. Pathway enrichment analysis was performed using the Gene Set Enrichment Analysis program (GSEA, v4.3.2, Broad Institute, MA, USA) for biological pathways obtained from the Molecular Signatures Database (MSigDB, Broad Institute, Human v2022.1, MA, USA). The preeclampsia gene-set was obtained from Moslehi et al[35]. GSEA parameters: 1000 permutations, weighted analysis. Gene set enrichment data were further clustered and visualised using the R package vissE with the parameters: computeMsigOverlap (thresh = 0.25), findMsigClusters (alg = cluster_walktrap, minSize =2)[55].

AUTHOR CONTRIBUTIONS

Designing research study: NS, JR, MA, LdN, AK. **Conducting experiments**: NS, JM, AN, LP, PZR, CMS, ETSS, LdN

Acquiring data: JM, AN, LP. **Analyzing data**: NS, IS, NM, AR, LM, GTB, FSFG, VC, AK. **Writing the manuscript**: all authors

ACKNOWLEGMENTS

This study was funded by the Queensland University of Technology ECR funds for AK, JR, MA, NS. The following authors are supported by fellowships from the NHMRC (AK – 1157741, GB - 2008542 and 1135898), US DOD (NS – PC190533). The authors thank Fred Hutch pathology (Miki Haraguchi & Stephanie Weaver) for histology assistance.

DATA AVAILABILITY

The data generated in this study are available in the Gene Expression Omnibus (GEO) under GSE223612.

CONFLICTS OF INTEREST

Andy Nam and Liuliu Pan are employed by Nanostring Technologies. Nicolas Matigian is employed by QCIF Bioinformatics.

REFERENCES

1. Bordt EA, Shook LL, Atyeo C, *et al.* Maternal SARS-CoV-2 infection elicits sexually dimorphic placental immune responses. *Sci Transl Med* 2021; **13**: eabi7428.
2. Edlow AG, Li JZ, Collier AY, *et al.* Assessment of Maternal and Neonatal SARS-CoV-2 Viral Load, Transplacental Antibody Transfer, and Placental Pathology in Pregnancies During the COVID-19 Pandemic. *JAMA Netw Open* 2020; **3**: e2030455.
3. Schwartz DA, Mulkey SB, Roberts DJ. SARS-CoV-2 Placentitis, Stillbirth and Maternal COVID-19 Vaccination: Clinical-Pathological Correlations. *Am J Obstet Gynecol* 2022.
4. Racicot K, Mor G. Risks associated with viral infections during pregnancy. *J Clin Invest* 2017; **127**: 1591-1599.
5. Palomo M, Youssef L, Ramos A, *et al.* Differences and similarities in endothelial and angiogenic profiles of preeclampsia and COVID-19 in pregnancy. *Am J Obstet Gynecol* 2022; **227**: 277 e271-277 e216.

6. Mendoza M, Garcia-Ruiz I, Maiz N, *et al.* Pre-eclampsia-like syndrome induced by severe COVID-19: a prospective observational study. *Bjog* 2020; **127**: 1374-1380.

7. Serrano B, Bonacina E, Garcia-Ruiz I, *et al.* Confirmation of preeclampsia-like syndrome induced by severe COVID-19: an observational study. *Am J Obstet Gynecol MFM* 2022; **5**: 100760.

8. Naeh A, Berezowsky A, Yudin MH, Dhalla IA, Berger H. Preeclampsia-Like Syndrome in a Pregnant Patient With Coronavirus Disease 2019 (COVID-19). *J Obstet Gynaecol Can* 2022; **44**: 193-195.

9. Celewicz A, Celewicz M, Michalczyk M, *et al.* SARS CoV-2 infection as a risk factor of preeclampsia and pre-term birth. An interplay between viral infection, pregnancy-specific immune shift and endothelial dysfunction may lead to negative pregnancy outcomes. *Ann Med* 2023; **55**: 2197289.

10. Gonzalez-Vanegas O, Martinez-Perez O. SARS-CoV-2 Infection and Preeclampsia-How an Infection Can Help Us to Know More about an Obstetric Condition. *Viruses* 2023; **15**.

11. Schwartz DA, Avvad-Portari E, Babál P, *et al.* Placental Tissue Destruction and Insufficiency From COVID-19 Causes Stillbirth and Neonatal Death From Hypoxic-Ischemic Injury. *Arch Pathol Lab Med* 2022; **146**: 660-676.

12. Huang C, Wang Y, Li X, *et al.* Clinical features of patients infected with 2019 novel coronavirus in Wuhan, China. *The Lancet* 2020; **395**: 497-506.

13. Maltepe E, Fisher SJ. Placenta: the forgotten organ. *Annu Rev Cell Dev Biol* 2015; **31**: 523-552.

14. Buchrieser J, Degrelle SA, Couderc T, *et al.* IFITM proteins inhibit placental syncytiotrophoblast formation and promote fetal demise. *Science* 2019; **365**: 176-180.

15. Wedenoja S, Yoshihara M, Teder H, *et al.* Fetal HLA-G mediated immune tolerance and interferon response in preeclampsia. *EBioMedicine* 2020; **59**: 102872.

16. Hamldar S, Kiani SJ, Khoshmirsafa M, *et al.* Expression profiling of inflammation-related genes including IFI-16, NOTCH2, CXCL8, THBS1 in COVID-19 patients. *Biologicals* 2022; **80**: 27-34.

17. Kulasinghe A, Tan CW, Ribeiro Dos Santos Miggiolaro AF, *et al.* Profiling of lung SARS-CoV-2 and influenza virus infection dissects virus-specific host responses and gene signatures. *Eur Respir J* 2022; **59**.

18. Conca W, Alabdely M, Albaiz F, *et al.* Serum beta2-microglobulin levels in Coronavirus disease 2019 (Covid-19): Another prognosticator of disease severity? *PLoS One* 2021; **16**: e0247758.

19. Jain NK, Tailang M, Jain HK, *et al.* Therapeutic implications of current Janus kinase inhibitors as anti-COVID agents: A review. *Front Pharmacol* 2023; **14**: 1135145.

20. Hu XQ, Zhang L. Hypoxia and Mitochondrial Dysfunction in Pregnancy Complications. *Antioxidants (Basel)* 2021; **10**.

21. Rana S, Burke SD, Karumanchi SA. Imbalances in circulating angiogenic factors in the pathophysiology of preeclampsia and related disorders. *Am J Obstet Gynecol* 2022; **226**: S1019-S1034.

22. Mukosera GT, Clark TC, Ngo L, *et al.* Nitric oxide metabolism in the human placenta during aberrant maternal inflammation. *J Physiol* 2020; **598**: 2223-2241.

23. Van Hove CE, Van der Donckt C, Herman AG, Bult H, Fransen P. Vasodilator efficacy of nitric oxide depends on mechanisms of intracellular calcium mobilization in mouse aortic smooth muscle cells. *Br J Pharmacol* 2009; **158**: 920-930.

24. Jansson T, Aye IL, Goberdhan DC. The emerging role of mTORC1 signaling in placental nutrient-sensing. *Placenta* 2012; **33 Suppl 2**: e23-29.

407 25. Hastie R, Brownfoot FC, Pritchard N, *et al.* EGFR (Epidermal Growth Factor
408 Receptor) Signaling and the Mitochondria Regulate sFlt-1 (Soluble FMS-Like
409 Tyrosine Kinase-1) Secretion. *Hypertension* 2019; **73**: 659-670.
410 26. Kramer AW, Lamale-Smith LM, Winn VD. Differential expression of human
411 placental PAPP-A2 over gestation and in preeclampsia. *Placenta* 2016; **37**: 19-25.
412 27. Neuman RI, Alblas van der Meer MM, Nieboer D, *et al.* PAPP-A2 and Inhibin A as
413 Novel Predictors for Pregnancy Complications in Women With Suspected or
414 Confirmed Preeclampsia. *J Am Heart Assoc* 2020; **9**: e018219.
415 28. Lamale-Smith LM, Gumina DL, Kramer AW, *et al.* Uteroplacental Ischemia Is
416 Associated with Increased PAPP-A2. *Reprod Sci* 2020; **27**: 529-536.
417 29. Guerby P, Tasta O, Swiader A, *et al.* Role of oxidative stress in the dysfunction of the
418 placental endothelial nitric oxide synthase in preeclampsia. *Redox Biol* 2021; **40**:
419 101861.
420 30. Karteris E, Vatish M, Hillhouse EW, Grammatopoulos DK. Preeclampsia is
421 associated with impaired regulation of the placental nitric oxide-cyclic guanosine
422 monophosphate pathway by corticotropin-releasing hormone (CRH) and CRH-related
423 peptides. *J Clin Endocrinol Metab* 2005; **90**: 3680-3687.
424 31. Ibanoglu MC, Oskovi-Kaplan ZA, Ozgu-Erdinc AS, Kara O, Sahin D. Comparison of
425 the Kisspeptin levels in early onset preeclampsia and late-onset preeclampsia. *Arch*
426 *Gynecol Obstet* 2022; **306**: 991-996.
427 32. Cruickshank T, MacDonald TM, Walker SP, *et al.* Circulating Growth Differentiation
428 Factor 15 Is Increased Preceding Preeclampsia Diagnosis: Implications as a Disease
429 Biomarker. *J Am Heart Assoc* 2021; **10**: e020302.

33. Kobayashi H, Matsubara S, Yoshimoto C, Shigetomi H, Imanaka S. Tissue Factor Pathway Inhibitors as Potential Targets for Understanding the Pathophysiology of Preeclampsia. *Biomedicines* 2023; **11**.

34. Nishizawa H, Pryor-Koishi K, Suzuki M, *et al.* Increased levels of pregnancy-associated plasma protein-A2 in the serum of pre-eclamptic patients. *Mol Hum Reprod* 2008; **14**: 595-602.

35. Moslehi R, Mills JL, Signore C, Kumar A, Ambroggio X, Dzutsev A. Integrative transcriptome analysis reveals dysregulation of canonical cancer molecular pathways in placenta leading to preeclampsia. *Sci Rep* 2013; **3**: 2407.

36. Aouache R, Biquard L, Vaiman D, Miralles F. Oxidative Stress in Preeclampsia and Placental Diseases. *Int J Mol Sci* 2018; **19**.

37. Redman CW, Staff AC. Preeclampsia, biomarkers, syncytiotrophoblast stress, and placental capacity. *Am J Obstet Gynecol* 2015; **213**: S9 e1, S9-11.

38. Mistry HD, Czajka AN, Kurlak LO, Pipkin FB, Taggart MJ, Tribe RT. Differential placental caveolin-1 gene expression in women with pre-eclampsia. *Archives of Disease in Childhood - Fetal and Neonatal Edition* 2011; **96**: Fa125-Fa126.

39. Nowicki B, Singhal J, Fang L, Nowicki S, Yallampalli C. Inverse relationship between severity of experimental pyelonephritis and nitric oxide production in C3H/HeJ mice. *Infect Immun* 1999; **67**: 2421-2427.

40. Ogando DG, Paz D, Cella M, Franchi AM. The fundamental role of increased production of nitric oxide in lipopolysaccharide-induced embryonic resorption in mice. *Reproduction* 2003; **125**: 95-110.

41. Kong L, Zhang Q, Chao J, *et al.* Polarization of macrophages induced by Toxoplasma gondii and its impact on abnormal pregnancy in rats. *Acta Trop* 2015; **143**: 1-7.

454 42. Wareing M, Bai X, Seghier F, *et al.* Expression and function of potassium channels in
455 the human placental vasculature. *Am J Physiol Regul Integr Comp Physiol* 2006; **291**:
456 R437-446.
457 43. Roberts JM, Rich-Edwards JW, McElrath TF, Garmire L, Myatt L, Global Pregnancy
458 C. Subtypes of Preeclampsia: Recognition and Determining Clinical Usefulness.
459 *Hypertension* 2021; **77**: 1430-1441.
460 44. Wagner PK, Otomo A, Christians JK. Regulation of pregnancy-associated plasma
461 protein A2 (PAPPA2) in a human placental trophoblast cell line (BeWo). *Reprod Biol*
462 *Endocrinol* 2011; **9**: 48.
463 45. Martinez C, Gonzalez-Ramirez J, Marin ME, *et al.* Isthmin 2 is decreased in
464 preeclampsia and highly expressed in choriocarcinoma. *Heliyon* 2020; **6**: e05096.
465 46. Sugulle M, Dechend R, Herse F, *et al.* Circulating and placental growth-
466 differentiation factor 15 in preeclampsia and in pregnancy complicated by diabetes
467 mellitus. *Hypertension* 2009; **54**: 106-112.
468 47. Hogg K, Blair JD, McFadden DE, von Dadelszen P, Robinson WP. Early onset pre-
469 eclampsia is associated with altered DNA methylation of cortisol-signalling and
470 steroidogenic genes in the placenta. *PLoS One* 2013; **8**: e62969.
471 48. Zheng L, Huang J, Su Y, Wang F, Kong H, Xin H. Overexpression of tissue factor
472 pathway inhibitor 2 attenuates trophoblast proliferation and invasion in preeclampsia.
473 *Hum Cell* 2020; **33**: 512-520.
474 49. Rebutini PZ, Zanchettin AC, Stonoga ETS, *et al.* Association Between COVID-19
475 Pregnant Women Symptoms Severity and Placental Morphologic Features. *Front*
476 *Immunol* 2021; **12**: 685919.

50. Khong TY, Mooney EE, Ariel I, *et al.* Sampling and Definitions of Placental Lesions: Amsterdam Placental Workshop Group Consensus Statement. *Arch Pathol Lab Med* 2016; **140**: 698-713.

51. Merritt CR, Ong GT, Church SE, *et al.* Multiplex digital spatial profiling of proteins and RNA in fixed tissue. *Nat Biotechnol* 2020; **38**: 586-599.

52. Jerby-Arnon L, Neftel C, Shore ME, *et al.* Opposing immune and genetic mechanisms shape oncogenic programs in synovial sarcoma. *Nat Med* 2021; **27**: 289-300.

53. Risso D, Ngai J, Speed TP, Dudoit S. Normalization of RNA-seq data using factor analysis of control genes or samples. *Nat Biotechnol* 2014; **32**: 896-902.

54. Ritchie ME, Phipson B, Wu D, *et al.* limma powers differential expression analyses for RNA-sequencing and microarray studies. *Nucleic Acids Res* 2015; **43**: e47.

55. Dharmesh D. Bhuva CWT, Ning Liu, Holly J. Whitfield, Nicholas Papachristos, Sam Lee, Malvika Kharbanda, Ahmed Mohamed, Melissa J. Davis. vissE: A versatile tool to identify and visualise higher-order molecular phenotypes from functional enrichment analysis. *bioRxiv* 2022.

TABLES AND FIGURE LEGENDS

Patient De-id.	Group	Sample Code	Participant Age	Gestational Age	Comorbidities	SARS-CoV-2 symptoms/ severity	Fetal sex	Fetal Outcome	Delivery Method	Fetal Weight (grams)	Placental Weight (grams)	Macroscopic observations
20-3594	SARS-CoV-2	2	25-30	30-35	Hypothyroidism and hypertensive disorder in pregnancy	+/+	Male	Preterm	na	2450	448	Infarcts and intervillous thrombosis (<5%)
20-3561	SARS-CoV-2	4	35-40	25-30	Hypothyroidism	+/+	Female	Preterm	C-section	na	245	-
20-3744	SARS-CoV-2	8	25-30	30-35	Gestational diabetes, bipolar disorder, hypothyroidism and syphilis (treated)	+/-	Female	Preterm	C-section	na	412	Infarcts (<5%)
20-5105	SARS-CoV-2	12	25-30	35-40	None	-	Female	Term	C-section	2960	462	-
20-3369	SARS-CoV-2	13	25-30	35-40	Gestational diabetes and hyperthyroidism	+/-	Female	Term	Assisted Vaginal	2600	358	Retroplacental and marginal hematoma, infarcts (<5%)
20-5869	SARS-CoV-2	18	25-30	35-40	None	+/-	Male	Term	C-section	2345	370	-
20-2916	SARS-CoV-2	22	20-25	35-40	None	-	Female	Term	Assisted Vaginal	3030	650	-
16-7859	CONTROL	1	20-25	30-35	Hypothyroidism		Male	Preterm	C-section	1180	270	Placental hypoplasia
18-13016	CONTROL	3	20-25	35-40	Hypothyroidism and hypertension		Female	Preterm	Assisted Vaginal	2223	498	-
16-8315	CONTROL	5	15-20	35-40	Obesity		Female	Term	Assisted Vaginal	3810	514	-
18-4906	CONTROL	9	20-25	25-30	None		Male	Preterm	Assisted Vaginal	1205	248	-
18-14057	CONTROL	10	40-45	30-35	Diabetes, hypertension, bipolar disorder		Male	Preterm	C-section	1650	243	Placental hypoplasia
16-7599	CONTROL	11	25-30	35-40	Gestational diabetes		Male	Term	C-section	3460	480	-
16-3340	CONTROL	15	35-40	35-40	None		Female	Term	C-section	3005	395	-
18-9951	CONTROL	16	20-25	35-40	None		Male	Term	C-section	3690	574	-
16-6144	CONTROL	19	25-30	35-40	None		Male	Term	C-section	3345	394	-

Table 1: Clinical information of the SARS-CoV-2 and control cohort

Figure 1: Study design and cell deconvolution. (a) 1. Placental cores collected at delivery from the SARS-CoV-2 (n=7) and control (n=9) groups were assembled into tissue microarray slides (TMAs). 2. TMAs were stained with fluorescent markers to differentiate cell types within anchoring (pink outline) and terminal villi (red outline). Barcodes were cleaved and collected from each region of interest by UV light. ***3.*** Cleaved barcodes were sequenced and counted using an Illumina® sequencer in preparation for transcriptomic analysis. Data were normalised before downstream differential expression analysis. **(b)** Transcriptional cell deconvolution map. **(c-j)** Box-plots of indicated cell type proportions from 1b. AV: anchoring villi, TV: terminal villi, SARS-CoV-2 group is n=7 and control group is n=9.

Figure 2: Enrichment of SARS-CoV-2 related pathways. **(a)** Principal component analysis of normalised gene counts from trophoblasts and villous core stromal compartments from SARS-CoV-2 (n=7) and control (n=9) groups at the anchoring or terminal villi (AV; TV). **(b)** Principal component dimensions. **(c)** Upset plot of differential gene expression in trophoblasts and villous core stromal compartments from the AV and TV in response to

SARS-CoV-2 infection. The bar charts on the left indicate the total number of differentially expressed genes for the indicated sample group and the bar charts on the top show the gene overlap for the comparisons indicated by the purple lines. Black dots denote differentially expressed genes that are unique for the indicated sample group. Fold change +/- 1.5, *P*-value <= 0.05, FDR < 0.05. **(d)** Enrichment of significant SARS-CoV-2 related pathways from the Reactome database, in the SARS-CoV-2 and control samples. Blue: significantly negatively enriched, red: significantly positively enriched, grey: not significant. The full list of enriched pathways from the Reactome database can be found in Supplementary table 2 and table 3. **(e)** Gene set enrichment analysis (GSEA) plot of the SARS_COV_2_INFECTION pathway from the Reactome database and **(f)** INTERFERON_ALPHA_RESPONSE from the Hallmark database, in SARS-CoV-2 samples versus controls. **(g-j)** Normalised expression counts of IFI27, B2M, JAK1, and STAT3 genes, in trophoblast (TB) or villous core stroma (VCS) compartments from the SARS-CoV-2 (n=7) and control samples (n=9). ** *P*-value < 0.01, *** *P*-value < 0.001.

Figure 3: Enrichment of placental dysfunction pathways with SARS-CoV-2. (a) Differentially enriched pathways form the Hallmarks database in trophoblasts (TB) and villous core stroma (VCS) compartments in SARS-CoV-2 (n=7) vs control group (n=9). Colour gradient refers to the normalised enrichment score. **(b)** Enriched gene ontology biological processes (GO-BP) pathway clusters from the Molecular Signatures Database (MSigDb) generated using vissE, in the VCS and **(c)** TB. Top row depicts upregulated pathways, bottom row depicts downregulated pathways. **(d)** Volcano plot of gene expression from VCS or **(e)** TB in response to SARS-CoV-2 infection. Fold change (FC) +/- 1.5, *P*-value <= 0.05, FDR < 0.05, the full list of differentially expressed genes can be found in Supplementary table 4. **(f-l)** Normalised expression counts of indicated genes in TB or VCS

compartments from the SARS-CoV-2 (n=7) and control samples (n=9). * *P*-value < 0.05, ** *P*-value < 0.01, *** *P*-value < 0.001, NS: not significant. **(m)** Gene set enrichment analysis (GSEA) plot of the preeclampsia signature generated by Moslehi et al, in SARS-CoV-2 samples versus controls.

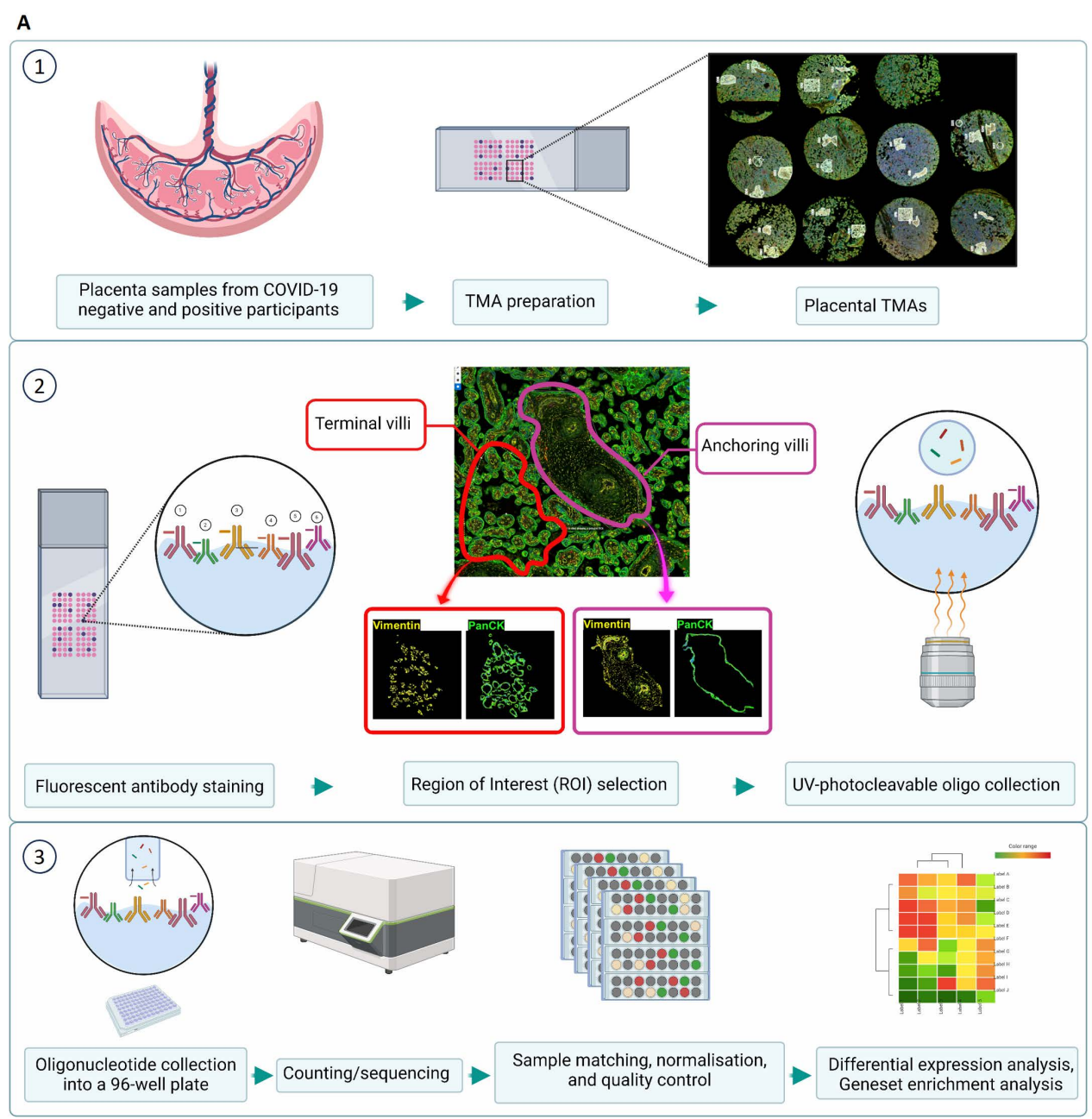
A
1
Placenta samples from COVID-19 negative and positive participants
TMA preparation
Placental TMAs
2
Terminal villi
Anchoring villi
Vimentin
PanCK
Vimentin
PanCK
Fluorescent antibody staining
Region of Interest (ROI) selection
UV-photocleavable oligo collection
3
Oligonucleotide collection into a 96-well plate
Counting/sequencing
Sample matching, normalisation, and quality control
Differential expression analysis, Geneset enrichment analysis

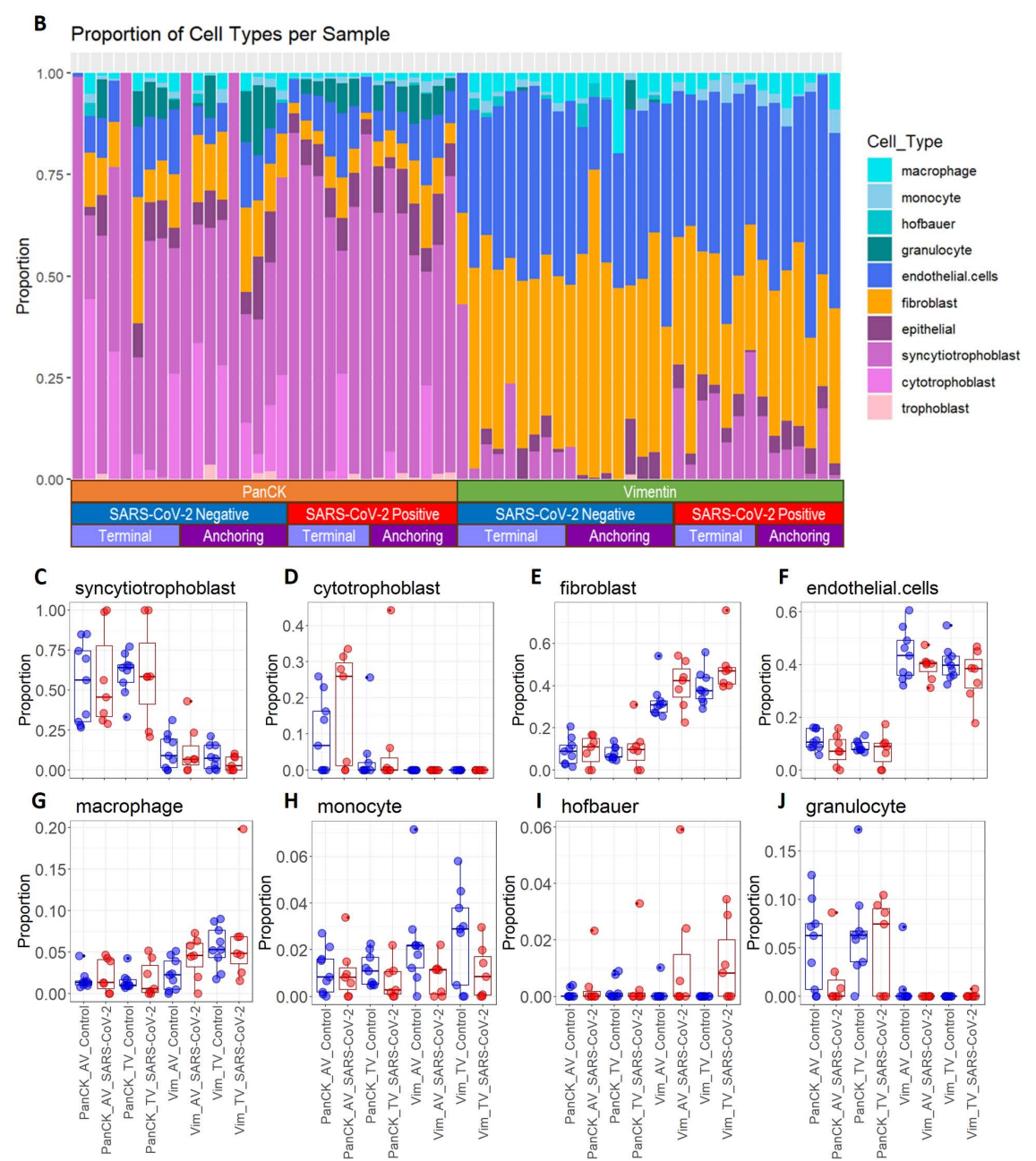
B
Proportion of Cell Types per Sample
Proportion
1.00
0.75
0.50
0.25
0.00
PanCK
Vimentin
SARS-CoV-2 Negative
SARS-CoV-2 Positive
SARS-CoV-2 Negative
SARS-CoV-2 Positive
Terminal
Anchoring
Terminal
Anchoring
Terminal
Anchoring
Terminal
Anchoring
Cell_Type
macrophage
monocyte
hofbauer
granulocyte
endothelial.cells
fibroblast
epithelial
syncytiotrophoblast
cytotrophoblast
trophoblast
C
syncytiotrophoblast
D
cytotrophoblast
E
fibroblast
F
endothelial.cells
G
macrophage
H
monocyte
I
hofbauer
J
granulocyte
PanCK_AV_Control
PanCK_AV_SARS-CoV-2
PanCK_TV_Control
PanCK_TV_SARS-CoV-2
Vim_AV_Control
Vim_AV_SARS-CoV-2
Vim_TV_Control
Vim_TV_SARS-CoV-2

Figure 1: Study design and cell deconvolution. (a) 1. Placental cores collected at delivery from the SARS-CoV-2 (n=7) and control (n=9) groups were assembled into tissue microarray slides (TMAs). 2. TMAs were stained with fluorescent markers to differentiate cell types within anchoring (pink outline) and terminal villi (red outline). Barcodes were cleaved and collected from each region of interest by UV light. ***3.*** Cleaved barcodes were sequenced and counted using an Illumina® sequencer in preparation for transcriptomic analysis. Data were normalised before downstream differential expression analysis. **(b)** Transcriptional cell deconvolution map. **(c-j)** Box-plots of indicated cell type proportions from 1b. AV: anchoring villi, TV: terminal villi, SARS-CoV-2 group is n=7 and control group is n=9.

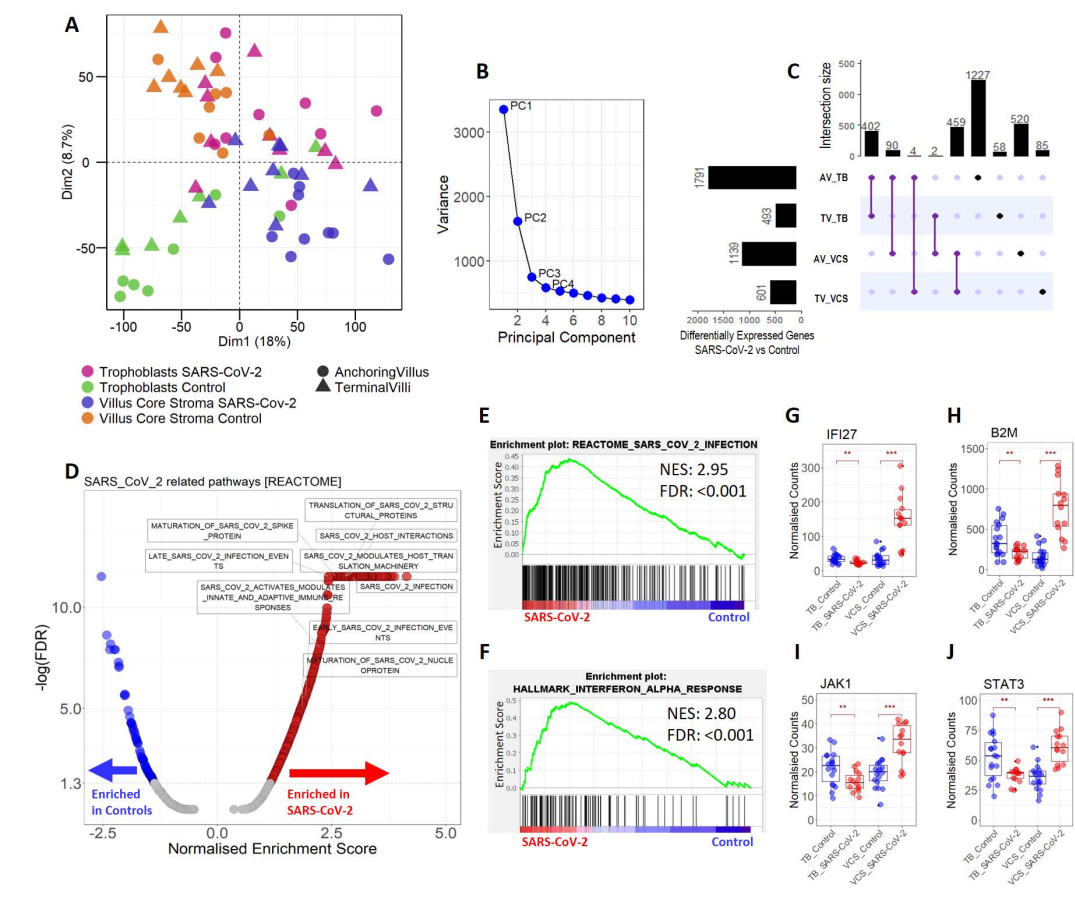
A
Dim2 (8.7%)
Dim1 (18%)
Trophoblasts SARS-CoV-2
Trophoblasts Control
Villus Core Stroma SARS-Cov-2
Villus Core Stroma Control
AnchoringVillus
TerminalVilli
B
Variance
Principal Component
PC1
PC2
PC3
PC4
C
Intersection size
AV_TB
TV_TB
AV_VCS
TV_VCS
Differentially Expressed Genes
SARS-CoV-2 vs Control
D
SARS_CoV_2 related pathways [REACTOME]
TRANSLATION_OF_SARS_COV_2_STRUCTURAL_PROTEINS
MATURATION_OF_SARS_COV_2_SPIKE_PROTEIN
SARS_COV_2_HOST_INTERACTIONS
LATE_SARS_COV_2_INFECTION_EVENTS
SARS_COV_2_MODULATES_HOST_TRANSLATION_MACHINERY
SARS_COV_2_ACTIVATES_MODULATES_INNATE_AND_ADAPTIVE_IMMUNE_RESPONSES
SARS_COV_2_INFECTION
EARLY_SARS_COV_2_INFECTION_EVENTS
MATURATION_OF_SARS_COV_2_NUCLEOPROTEIN
-log(FDR)
Enriched in Controls
Enriched in SARS-CoV-2
Normalised Enrichment Score
E
Enrichment plot: REACTOME_SARS_COV_2_INFECTION
Enrichment Score
NES: 2.95
FDR: <0.001
SARS-CoV-2
Control
F
Enrichment plot:
HALLMARK_INTERFERON_ALPHA_RESPONSE
NES: 2.80
FDR: <0.001
SARS-CoV-2
Control
G
IFI27
Normalised Counts
TB_Control
TB_SARS-CoV-2
VCS_Control
VCS_SARS-CoV-2
H
B2M
I
JAK1
J
STAT3

Figure 2: Enrichment of SARS-CoV-2 related pathways. **(a)** Principal component analysis of normalised gene counts from trophoblasts and villous core stromal compartments from SARS-CoV-2 (n=7) and control (n=9) groups at the anchoring or terminal villi (AV; TV). **(b)** Principal component dimensions. **(c)** Upset plot of differential gene expression in trophoblasts and villous core stromal compartments from the AV and TV in response to SARS-CoV-2 infection. The bar charts on the left indicate the total number of differentially expressed genes for the indicated sample group and the bar charts on the top show the gene overlap for the comparisons indicated by the purple lines. Black dots denote differentially expressed genes that are unique for the indicated sample group. Fold change +/- 1.5, *P*-value <= 0.05, FDR < 0.05. (**d)** Enrichment of significant SARS-CoV-2 related pathways from the Reactome database, in the SARS-CoV-2 and control samples. Blue: significantly negatively enriched, red: significantly positively enriched, grey: not significant. The full list of enriched pathways from the Reactome database can be found in Supplementary table 2 and table 3. **(e)** Gene set enrichment analysis (GSEA) plot of the SARS_COV_2_INFECTION pathway from the Reactome database and **(f)** INTERFERON_ALPHA_RESPONSE from the Hallmark database, in SARS-CoV-2 samples versus controls. **(g-j)** Normalised expression counts of IFI27, B2M, JAK1, and STAT3 genes, in trophoblast (TB) or villous core stroma (VCS) compartments from the SARS-CoV-2 (n=7) and control samples (n=9). ** *P*-value < 0.01, *** *P*-value < 0.001.

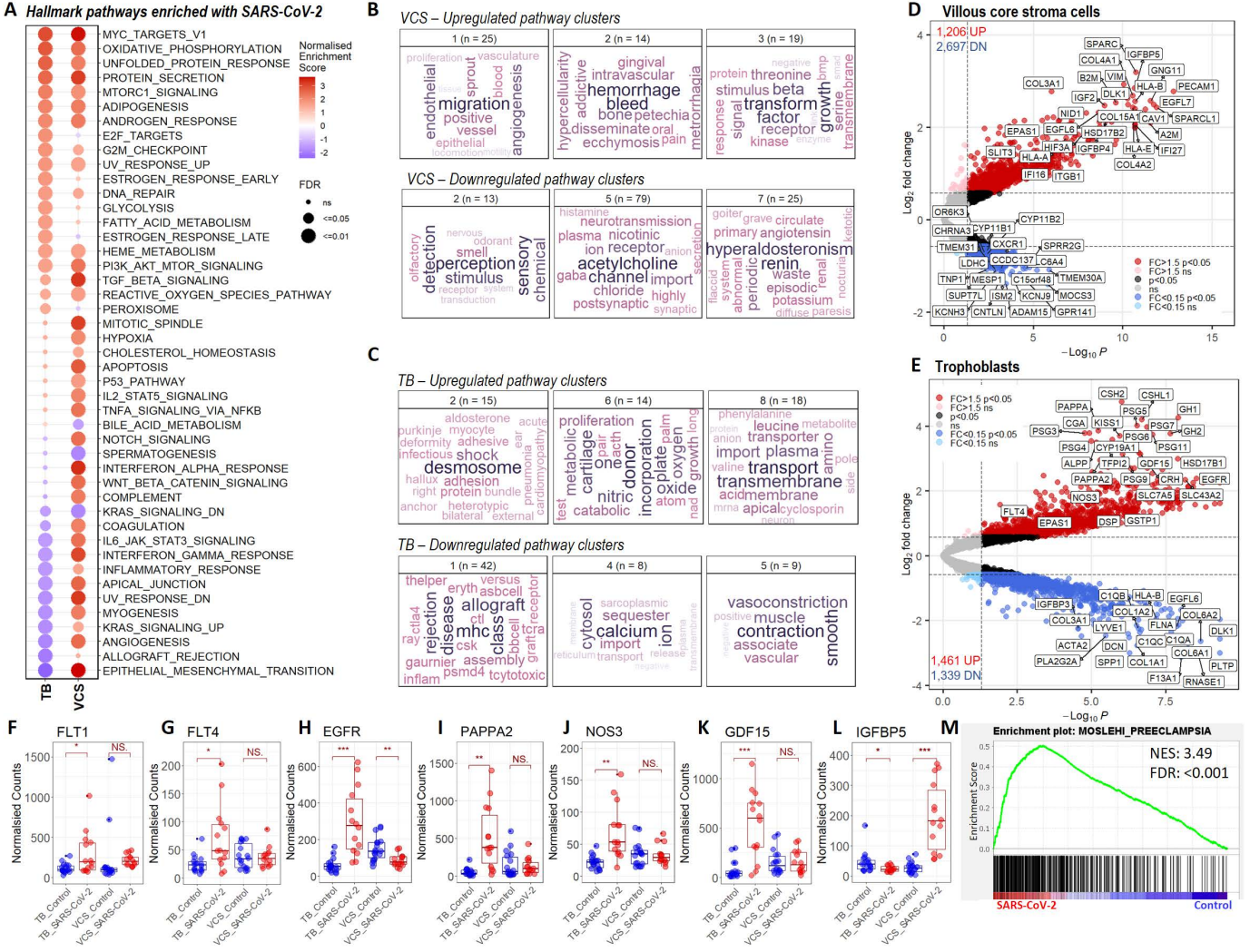
A
Hallmark pathways enriched with SARS-CoV-2
MYC_TARGETS_V1
OXIDATIVE_PHOSPHORYLATION
UNFOLDED_PROTEIN_RESPONSE
PROTEIN_SECRETION
MTORC1_SIGNALING
ADIPOGENESIS
ANDROGEN_RESPONSE
E2F_TARGETS
G2M_CHECKPOINT
UV_RESPONSE_UP
ESTROGEN_RESPONSE_EARLY
DNA_REPAIR
GLYCOLYSIS
FATTY_ACID_METABOLISM
ESTROGEN_RESPONSE_LATE
HEME_METABOLISM
PI3K_AKT_MTOR_SIGNALING
TGF_BETA_SIGNALING
REACTIVE_OXYGEN_SPECIES_PATHWAY
PEROXISOME
MITOTIC_SPINDLE
HYPOXIA
CHOLESTEROL_HOMEOSTASIS
APOPTOSIS
P53_PATHWAY
IL2_STAT5_SIGNALING
TNFA_SIGNALING_VIA_NFKB
BILE_ACID_METABOLISM
NOTCH_SIGNALING
SPERMATOGENESIS
INTERFERON_ALPHA_RESPONSE
WNT_BETA_CATENIN_SIGNALING
COMPLEMENT
KRAS_SIGNALING_DN
COAGULATION
IL6_JAK_STAT3_SIGNALING
INTERFERON_GAMMA_RESPONSE
INFLAMMATORY_RESPONSE
APICAL_JUNCTION
UV_RESPONSE_DN
MYOGENESIS
KRAS_SIGNALING_UP
ANGIOGENESIS
ALLOGRAFT_REJECTION
EPITHELIAL_MESENCHYMAL_TRANSITION
TB
VCS
Normalised Enrichment Score
3
2
1
0
-1
-2
FDR
ns
<=0.05
<=0.01
B
VCS – Upregulated pathway clusters
1 (n = 25)
2 (n = 14)
3 (n = 19)
VCS – Downregulated pathway clusters
2 (n = 13)
5 (n = 79)
7 (n = 25)
C
TB – Upregulated pathway clusters
2 (n = 15)
6 (n = 14)
8 (n = 18)
TB – Downregulated pathway clusters
1 (n = 42)
4 (n = 8)
5 (n = 9)
D
Villous core stroma cells
1,206 UP
2,697 DN
Log2 fold change
−Log10 P
FC>1.5 p<0.05
FC>1.5 ns
p<0.05
ns
FC<0.15 p<0.05
FC<0.15 ns
E
Trophoblasts
1,461 UP
1,339 DN
Log2 fold change
−Log10 P
FC>1.5 p<0.05
FC>1.5 ns
p<0.05
ns
FC<0.15 p<0.05
FC<0.15 ns
F
FLT1
G
FLT4
H
EGFR
I
PAPPA2
J
NOS3
K
GDF15
L
IGFBP5
Normalised Counts
NS.
TB_Control
TB_SARS-CoV-2
VCS_Control
VCS_SARS-CoV-2
M
Enrichment plot: MOSLEHI_PREECLAMPSIA
NES: 3.49
FDR: <0.001
Enrichment Score
SARS-CoV-2
Control

Figure 3: Enrichment of placental dysfunction pathways with SARS-CoV-2.

(a) Differentially enriched pathways form the Hallmarks database in trophoblasts (TB) and villous core stroma (VCS) compartments in SARS-CoV-2 (n=7) vs control group (n=9). Colour gradient refers to the normalised enrichment score. **(b)** Enriched gene ontology biological processes (GO-BP) pathway clusters from the Molecular Signatures Database (MSigDb) generated using vissE, in the VCS and **(c)** TB. Top row depicts upregulated pathways, bottom row depicts downregulated pathways. **(d)** Volcano plot of gene expression from VCS or **(e)** TB in response to SARS-CoV-2 infection. Fold change (FC) +/- 1.5, *P*-value <= 0.05, FDR < 0.05, the full list of differentially expressed genes can be found in Supplementary table 4. **(f-l)** Normalised expression counts of indicated genes in TB or VCS compartments from the SARS-CoV-2 (n=7) and control samples (n=9). * *P*-value < 0.05, ** *P*-value < 0.01, *** *P*-value < 0.001, NS: not significant. **(m)** Gene set enrichment analysis (GSEA) plot of the preeclampsia signature generated by Moslehi et al, in SARS-CoV-2 samples versus controls.

Patient De-id.	Group	Sample Code	Participant Age	Gestational Age	Comorbidities	SARS-CoV-2 symptoms/ severity	Fetal sex	Fetal Outcome	Delivery Method	Fetal Weight (grams)	Placental Weight (grams)	Macroscopic observations
20-3594	SARS-CoV-2	2	25-30	30-35	Hypothyroidism and hypertensive disorder in pregnancy	+/+	Male	Preterm	na	2450	448	Infarcts and intervillous thrombosis (<5%)
20-3561	SARS-CoV-2	4	35-40	25-30	Hypothyroidism	+/+	Female	Preterm	C-section	na	245	-
20-3744	SARS-CoV-2	8	25-30	30-35	Gestational diabetes, bipolar disorder, hypothyroidism and syphilis (treated)	+/-	Female	Preterm	C-section	na	412	Infarcts (<5%)
20-5105	SARS-CoV-2	12	25-30	35-40	None	-	Female	Term	C-section	2960	462	-
20-3369	SARS-CoV-2	13	25-30	35-40	Gestational diabetes and hyperthyroidism	+/-	Female	Term	Assisted Vaginal	2600	358	Retroplacental and marginal hematoma, infarcts (<5%)
20-5869	SARS-CoV-2	18	25-30	35-40	None	+/-	Male	Term	C-section	2345	370	-
20-2916	SARS-CoV-2	22	20-25	35-40	None	-	Female	Term	Assisted Vaginal	3030	650	-
16-7859	CONTROL	1	20-25	30-35	Hypothyroidism		Male	Preterm	C-section	1180	270	Placental hypoplasia
18-13016	CONTROL	3	20-25	35-40	Hypothyroidism and hypertension		Female	Preterm	Assisted Vaginal	2223	498	-
16-8315	CONTROL	5	15-20	35-40	Obesity		Female	Term	Assisted Vaginal	3810	514	-
18-4906	CONTROL	9	20-25	25-30	None		Male	Preterm	Assisted Vaginal	1205	248	-
18-14057	CONTROL	10	40-45	30-35	Diabetes, hypertension, bipolar disorder		Male	Preterm	C-section	1650	243	Placental hypoplasia
16-7599	CONTROL	11	25-30	35-40	Gestational diabetes		Male	Term	C-section	3460	480	-
16-3340	CONTROL	15	35-40	35-40	None		Female	Term	C-section	3005	395	-
18-9951	CONTROL	16	20-25	35-40	None		Male	Term	C-section	3690	574	-
16-6144	CONTROL	19	25-30	35-40	None		Male	Term	C-section	3345	394	-

Table 1: Clinical information of the SARS-CoV-2 and control cohort